

Breaking the Warp Barrier: Hyper-Fast Solitons in Einstein-Maxwell-Plasma Theory

Erik W. Lenz

Institut für Astrophysik, Georg-August Universität Göttingen, Göttingen, Germany
37077

E-mail: erik.lenz@uni-goettingen.de

15 June 2020

Abstract. Solitons in space-time capable of transporting time-like observers at superluminal speeds have long been tied to violations of the weak, strong, and dominant energy conditions of general relativity. The negative-energy sources required for these solitons must be created through energy-intensive uncertainty principle processes as no such classical source is known in particle physics. This paper overcomes this barrier by constructing a class of soliton solutions that are capable of superluminal motion and sourced by purely positive energy densities. The solitons are also shown to be capable of being sourced from the stress-energy of a conducting plasma and classical electromagnetic fields. This is the first example of hyper-fast solitons resulting from known and familiar sources, reopening the discussion of superluminal mechanisms rooted in conventional physics.

1. Introduction

Hyper-fast solitons within modern theories of gravity have been a topic of energetic speculation in recent decades [1, 2, 3, 4, 5, 6, 7, 8, 9, 10, 11, 12, 13, 14, 15, 16, 17, 18]. One of the most prominent critiques of compact mechanisms of superluminal motion within general relativity is that the geometry must largely be sourced from a form of negative energy density, though there are no such known macroscopic sources in particle physics. Other concerns include difficulties associated with constructing a soliton from a nearly flat space-time up to the superluminal phase, where the transported central observers become surrounded by a horizon, and the equal difficulties of evolving from the superluminal phase back the flat space-time. Challenges associated with creating horizons also include communication between inside and outside observers through the soliton shell, bombardment of the inside observers by Hawking radiation, and stress-energy buildup on the leading horizon. Further, creating an Alcubierre-type superluminal soliton would need an immense amount of (magnitude) energy, in excess of the scale that is in the visible universe, $E_{tot} \sim -6 \times 10^{62} v_s/c$ kg mass equivalent [3], though some progress has been made in this area, reducing the required energy to

$\sim -10^{28}v_s/c$ kg mass equivalent [7], and even down to $\sim -10^3v_s/c$ kg mass equivalent with additional speculative assumptions [16, 17].

This paper addresses the first critique by constructing a new class of hyper-fast soliton solutions within general relativity that are sourced purely from positive energy densities, thus removing the need for exotic negative-energy-density sources. This is made possible through considering hyperbolic relations between components of the space–time metric’s shift vector, which depart from the elliptical or linear relations that limited solitons in the previous literature to require negative energies. Further, these solutions are sourceable by a classical electronic plasma, placing superluminal phenomena into the purview of known physics. The remainder of the paper is structured as follows: Section 2 presents the geometry of these solitons using the ADM formalism [19] and the components of the Einstein equation relevant for the class of solutions; Section 3 introduces the conditions of the hyperbolically-related shift vectors and the rules for constructing a class of solutions with everywhere-positive energy density and standard energy-momentum conditions and demonstrates these qualities for a family of solutions; Section 4 solves the dynamics of the geometry via the Einstein equation trace and derives requirements on the sourcing plasma; and Section 5 discusses the consequences of discovering a superluminal mechanism driven by known sources and potential avenues for future study.

2. Solitons in General Relativity

The space–times considered here are decomposed in the “3+1” (ADM) formalism using a similar convention to that presented in [20], or [21], specifically following the later’s sign protocol. The line element of the space–time is cast in the form

$$ds^2 = - (N^2 - N^i N_i) dt^2 - 2N_i dx^i dt + h_{ij} dx^i dx^j, \quad (1)$$

where the time coordinate t stratifies space–time into space-like hypersurfaces, the space metric components h_{ij} evaluated at t provide the intrinsic geometry of that hypersurface, and the similarly-evaluated shift vector components N^i at t provide the coordinate three-velocity of the hypersurface’s normal. The time-like unit normal one-form is therefore proportional to the coordinate time element $\mathbf{n}^* = N dt$, and the unit normal vector \mathbf{n} to the hypersurface has components

$$n^\nu = \left(\frac{1}{N}, \frac{N^i}{N} \right). \quad (2)$$

Einstein summation notation is used throughout this paper, with Greek indices running over space–time components and Latin indices over space components. The lowering of Latin indices is performed using the hypersurface metric h unless otherwise stated. Natural units $G = c = 1$ are used. Lastly, the lapse function N is set to unity.

Central to the computation of the Einstein tensor is the hypersurface extrinsic curvature, which can be written as the negative covariant derivative of the normal

vector field \mathbf{n} , or in terms of coordinate derivatives as

$$K_{ij} = -\frac{1}{2} (\partial_t h_{ij} + N^k \partial_k h_{ij} + \partial_i N^k h_{kj} + \partial_j N^k h_{ki}). \quad (3)$$

The solutions considered here will have hypersurfaces parameterized by flat metrics under Cartesian coordinates $h_{ij} = \delta_{ij}$, reducing the extrinsic curvature expression to the symmetric combination of shift vector derivatives. The trivial form of N and h imply that the Eulerian observers, that is time-like observers whose motion in space-time is normal to the hypersurfaces with four-velocity \mathbf{n} , are in free fall.

Resolving the behavior of solitons within general relativity begins with a check of the weak energy condition and the momentum conditions. The weak energy condition is given by the projection of the Einstein equation onto the hypersurface normal

$$G^{\mu\nu} n_\mu n_\nu = \left(R^{\mu\nu} - \frac{1}{2} g^{\mu\nu} R \right) n_\mu n_\nu = 8\pi T^{\mu\nu} n_\mu n_\nu, \quad (4)$$

where the projected stress-energy is to be called the local Eulerian energy density

$$T^{\mu\nu} n_\mu n_\nu = N^2 T^{00} = E. \quad (5)$$

The geometric side of the energy constraint equation is divisible into the intrinsic hypersurface curvature ${}^{(3)}R$ and the extrinsic curvature's trace $K = K_i^i$ and its quadratic hypersurface scalar $K_j^i K_i^j$

$$8\pi E = \frac{1}{2} ({}^{(3)}R - K_j^i K_i^j + K^2). \quad (6)$$

The contribution of hypersurface intrinsic curvature to the energy vanishes in the presence of the flat space metric h . The purely geometric portion of the energy condition may be further expanded in terms of the shift vector components

$$\begin{aligned} K^2 - K_j^i K_i^j &= 2\partial_x N_x \partial_y N_y + 2\partial_x N_x \partial_z N_z + 2\partial_z N_z \partial_y N_y \\ &\quad - \frac{1}{2} (\partial_x N_y + \partial_y N_x)^2 - \frac{1}{2} (\partial_x N_z + \partial_z N_x)^2 - \frac{1}{2} (\partial_z N_y + \partial_y N_z)^2. \end{aligned} \quad (7)$$

Note that the last three elements of the expression are negative definite, while the first three are of indeterminant type. These first three terms have the potential to provide the energy functional with an island of configurations that satisfy the weak energy condition. The first task of this work will be to show there exist non-flat moving compact configurations that have everywhere positive energy.

The momentum conditions are implemented here by comparing the mixed projection local Eulerian momentum density,

$$J_i = -n_\alpha T_i^\alpha = NT_i^0, \quad (8)$$

to the mixed projection of the Einstein tensor, resulting in the three conditions for the considered geometries

$$8\pi J_i = \partial_j K_i^j - \partial_i K. \quad (9)$$

Both the energy and momentum conditions must be satisfied everywhere and will provide a sense for the sources needed to construct the soliton geometries.

The dynamics of the geometry are in general set by the remaining six free components of the Einstein equation. Several of these degrees have already been made moot by the choice of a flat h and constant lapse function N . The conditions for positive energy solutions introduced in the next section will reduce the number of dynamical geometric degrees of freedom to one, meaning that only a single component of the dynamical portion of the Einstein equation is needed. The trace condition is a natural choice, given by

$$8\pi T_\mu^\mu = -2R, \quad (10)$$

where the space–time Ricci scalar decomposes in this class of space–times as

$$R = K^2 + K_i^i K_i^j + 2\mathcal{L}_n K, \quad (11)$$

where $\mathcal{L}_n()$ is the Lie derivative in the direction of the normal unit vector field.

3. Constructing Positive-Energy Solutions Using a Hyperbolic Shift Vector Potential

The class of geometries studied here will be characterized by a shift vector potential function, a real-valued function ϕ with spatial gradient relating the shift vector components

$$N_i = \partial_i \phi. \quad (12)$$

The soliton potentials will further be set to a steady state, moving with constant velocity and allowing the potential to be parameterized by displacement from its moving center $\phi(x - x_s(t), y - y_s(t), z - z_s(t))$, and $\dot{x}_s(t) = v_x$, $\dot{y}_s(t) = v_y$, and $\dot{z}_s(t) = v_z$ are the constant velocity components of the soliton.

The potential condition alone is insufficient to produce a positive definite functional of Eqn. 7, and so a relation between all the shift vector components is added. The most common relations explored in the literature are linear and elliptical. Specifically, the linear relation ($N_x = N_y = 0$) of [1] produced the renowned toroid of negative energy density, here displayed in Cartesian coordinates,

$$E_{\text{Alc}} = \frac{-1}{32\pi} ((\partial_x N_z)^2 + (\partial_y N_z)^2). \quad (13)$$

The expansionless ($K = -1/2(\partial_x N_x + \partial_y N_y + \partial_z N_z) = 0$) elliptical relation of [11] restricted the energy form to the negative definite square of the extrinsic curvature

$$E_{\text{Nat}} = \frac{-1}{16\pi} K_j^i K_i^j. \quad (14)$$

Parabolic and hyperbolic relations remained to be explored.

The hyperbolic relation is examined here. Specifically, the potential function will be taken to satisfy a linear wave equation over the spatial coordinates

$$\partial_x^2\phi + \partial_y^2\phi - \frac{2}{v_h^2}\partial_z^2\phi = \rho, \quad (15)$$

where $v_h/\sqrt{2}$ is the dimensionless wave front ‘speed’ on the hypersurface, and ρ is the source function. The positive z -axis is singled out as it will be the principal direction of travel for the soliton. Therefore, the remainder of this paper will consider only motion along the z direction, setting $v_x = v_y = 0$. The geometric side of the energy condition can then be rewritten as

$$\begin{aligned} K^2 - K_j^i K_i^j &= 2\partial_x^2\phi\partial_y^2\phi + 2\partial_z^2\phi \left(\frac{2}{v_h^2}\partial_z^2\phi + \rho \right) \\ &\quad - 2(\partial_y\partial_x\phi)^2 - 2(\partial_z\partial_x\phi)^2 - 2(\partial_y\partial_z\phi)^2. \end{aligned} \quad (16)$$

It is not altogether clear what the sign of the energy functional is, so two simplifications are applied. Assuming that ρ and ϕ are both parameterized in the (x, y) coordinates by the l_1 norm $s = |x| + |y|$, the energy further can be further simplified to a two-coordinate form, here using (z, x) ,

$$E = \frac{1}{16\pi} \left(2\partial_z^2\phi \left(\rho + \frac{2}{v_h^2}\partial_z^2\phi \right) - 4(\partial_z\partial_x\phi)^2 \right). \quad (17)$$

The Green’s function representation of the potential, holding that the potential’s initial condition at $z \rightarrow -\infty$ is null, takes the form

$$\phi = \int dx' dz' \frac{1}{4v_h} \Theta \left(z - z' - \frac{|\Delta x|}{v_h} \right) \rho(z', |x'| + |y|), \quad (18)$$

where $\Theta()$ is the Heaviside function, $\Delta x = x - x'$. The shift vectors can then be found in the Green’s form

$$N_z = \frac{1}{4v_h} \int dx' \rho \left(z - \frac{|\Delta x|}{v_h}, |x'| + |y| \right), \quad (19)$$

$$N_x = -\frac{1}{4v_h^2} \int dx' \text{sign}(\Delta x) \rho \left(z - \frac{|\Delta x|}{v_h}, |x'| + |y| \right), \quad (20)$$

where $\text{sign}()$ is the sign function. One can see that the shift vectors are proportional to integrals of source over the ‘past’ wave cone. Given the Green’s expressions, it can be straightforwardly computed that $|\partial_z^2\phi| \geq v_h|\partial_z\partial_x\phi|$, implying that the energy condition satisfies the inequality

$$\begin{aligned} E &\geq 2\rho \times \partial_z^2\phi \\ &= \rho \times \frac{1}{2v_h} \int dx' \partial_r \rho(r, |x'| + |y|) |_{r=z-|\Delta x|/v_h}, \end{aligned} \quad (21)$$

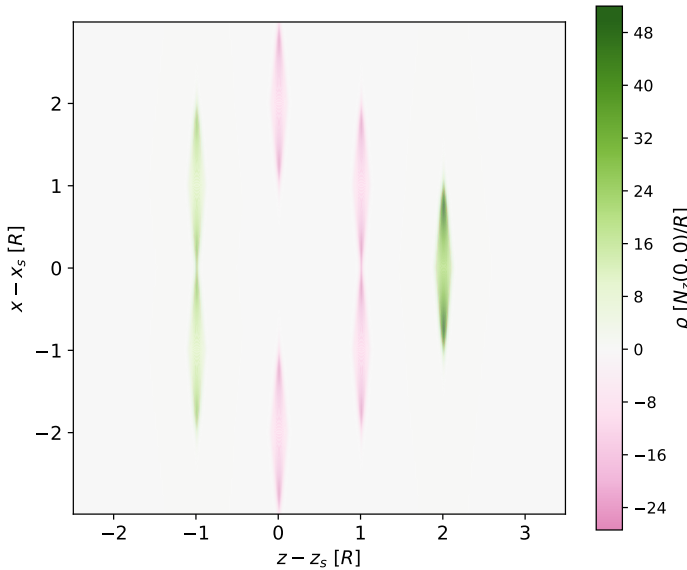


Figure 1. Projection of the source ρ of shift vector potential ϕ along $(x, 0, z)$. Propagation direction of the soliton is along the z -axis. Charge within each chord perpendicular to the long axis of the sources are calibrated to give a level surface in the central region. Shape and charge profile of each rhomboid source are identical. Total integrated charge of the system is 0.

from which rules may be formed to ensure the energy density is everywhere positive. For instance, the energy function will be positive definite for configurations such that the local source density and the z -component source density gradient integrated along the intersecting ‘past’ wave trajectories are of the same sign.

Consider the pentagonal configuration of sources in Fig. 1, illustrated via bi-lateral s -projection onto the $(x, 0, z)$ plane of a hypersurface, as a demonstration of one such compact positive energy configuration with net motion $v_z = v_s$. The configuration is such that the spatial wave fronts traveling from the left-most beams create a broad region of high and level N_z at the center, terminating on the right-most pair of beams of opposing density, with the remaining sources organized to terminate the stray branches of the wave cone, Fig. 2. The sources are formed as rhomboids in the 2D projection such that the boundary lines are angled to be between the surface of the hyperbolic wavefront cone and the z -constant plane. The perpendicular components of the shift vector are seen to vanish in the central region, while the parallel component over the same region is also very level but non-zero, a nearly tidal force free environment for a craft. The soliton center is a placid region where Eulerian observers move along essentially straight lines at $v_{rel} = N_z(0) - v_s$ relative to the soliton. This is in contrast to the volatile boundary where shifts can be much greater in size and variable in direction. The relation between N_z and v_s is derived from the trace dynamics in the next section.

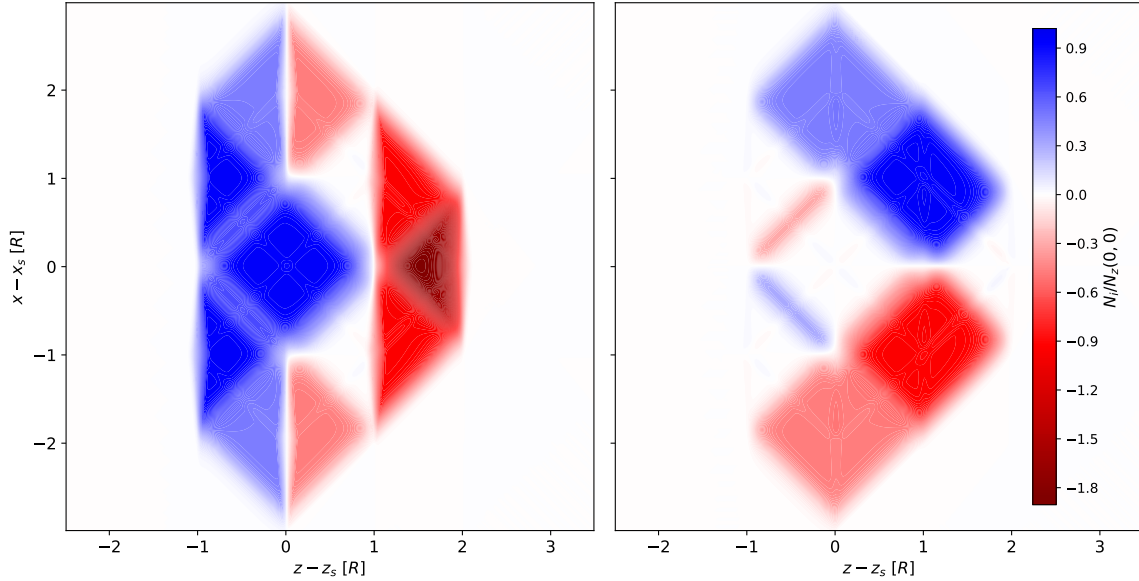


Figure 2. Projection of the shift vector components N_z (left) and N_x (right) along $(x, 0, z)$. Propagation direction of the soliton is from left to right along the z -axis.

The energy density of the soliton is seen to be positive definite in Fig. 3. Each rhomboid source ρ_{rhomb} is constructed individually to be everywhere positive and to be positive in the presence of other similar individual sources of ρ_{rhomb} . One can therefore piece together many other solutions from these elements of hyperbolic source. The total energy requirements of the positive-energy solitons closely follow that of [3] as applied to the Alcubierre solution

$$E_{\text{tot}} = \int E \sqrt{-g} d^3x. \quad (22)$$

For solitons where the extent of the central region R is much larger than the thickness of the boundary shell w ($w \ll R$), the energy is estimated to be

$$E_{\text{tot}} \sim Cv_s^2 \frac{R^2}{w} \quad (23)$$

where C is a form factor typically of order unity. The required energy for a soliton of $R = 100$ m and $w = 1$ m approaches a mass equivalent of $E_{\text{tot}} \sim (\text{few}) \times 10^{-1} M_\odot v_s$, which is of the magnitude as the estimate of [3] for an Alcubierre solution of the same dimensions, but without the uncertainties associated with where one might source the energy. The estimate for the Alcubierre solution sourced by naturally occurring Casimir forces is much higher, $\sim -6 \times 10^{62} v_s$ kg, which requires one to reduce the boundary thickness to a few hundred Planck lengths. However, no such naturality conditions are known to restrict the classical plasma driving the positive energy solutions. Further, many soliton solutions have been made since [1] that drastically improved on the overall

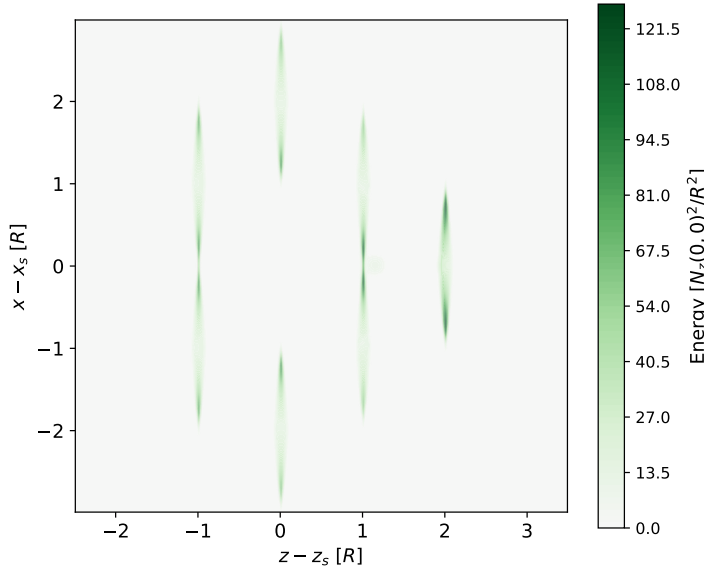


Figure 3. Projection of the local energy density of Eqn. 17 along $(x, 0, z)$. Propagation direction of the soliton is from left to right along the z -axis. The energy density is dominated by those regions containing hyperbolic source ρ , but also extends weakly to the boundaries of the wavefronts. The energy density is everywhere positive and therefore satisfies the weak energy condition.

negative energy requirements [7, 10, 16, 17]. Several of these approaches may provide proportional savings in energy for the positive-energy soliton.

The hypersurface volume expansion, calculated here from the extrinsic curvature trace $\theta = K$, can be found in Fig. 4. The volume expansion of the positive-energy soliton is complex, containing multiple positive and negative lobes associated with negative and positive hyperbolic source respectively, whereas the solution of [1] possesses only one negative expansion lobe at the leading edge of its soliton and one positive expansion lobe at the trailing edge. Both solutions have net expansion of 0.

The momentum conditions under the hyperbolic shift vector potential can be expressed as a gradient of the extrinsic curvature trace or equivalently in terms of the hyperbolic potential and source

$$\begin{aligned} J_i &= \frac{1}{8\pi} \partial_i K \\ &= \frac{1}{8\pi} \partial_i \left(\rho + \left(1 + \frac{2}{v_h^2} \right) \partial_z^2 \phi \right). \end{aligned} \quad (24)$$

The momentum density traces the edges of the energy dense regions, indicating circulation at the boundaries, Fig. 5. The relative fraction of momentum to energy remains between 0 and 1, indicating that the stress-energy source has an energy-momentum relation satisfiable by an electric plasma consisting of a massive fluid and

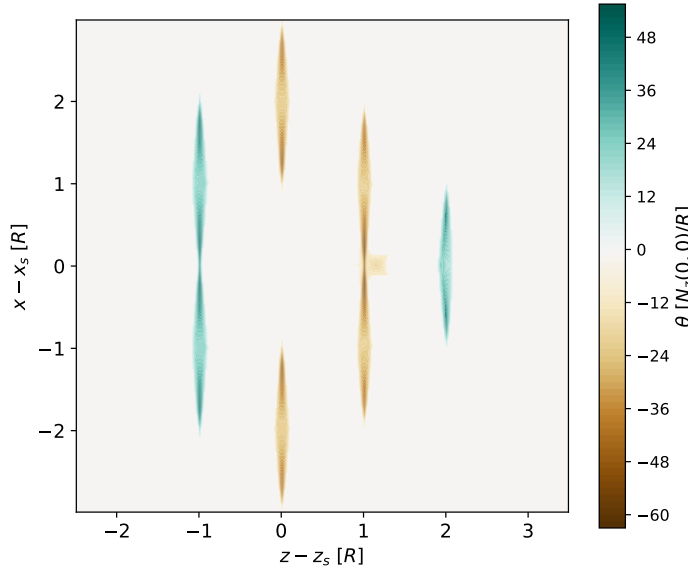


Figure 4. Projection of the local volume expansion factor θ along $(x, 0, z)$. Propagation direction of the soliton is from left to right along the z -axis.

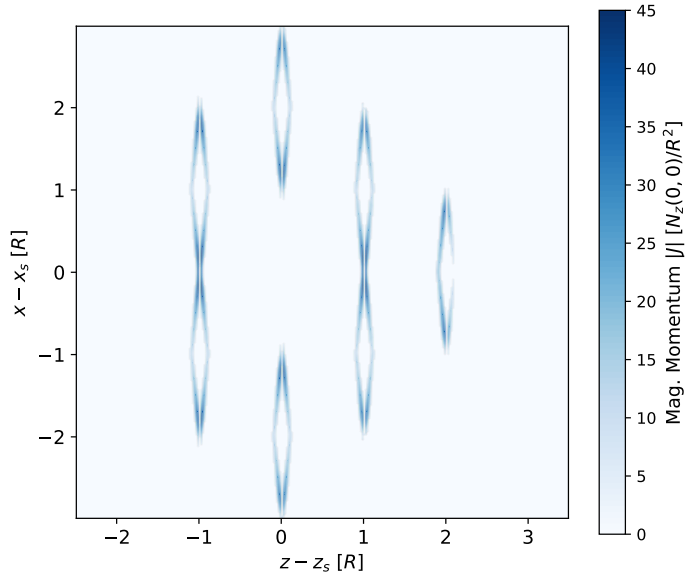


Figure 5. Projection of the local magnitude momentum density of Eqn. 24 along $(x, 0, z)$. Propagation direction of the soliton is from left to right along the z -axis. The momentum density traces the boundaries of the energy density.

electromagnetic fields.

4. Soliton-Plasma Dynamics

This section describes the conditions needed for an electrically conducting plasma to act as source for the positive-energy soliton. The dynamics of the hyperbolic potential ϕ , or equivalently the hyperbolic source ρ , can be set by the Einstein equation trace, Eqn. 10. The Ricci scalar under the conditions of the previous section becomes

$$R = -16\pi E + 2\theta^2 + 16\pi ((N_z - v_s) J_z + 2N_x J_x). \quad (25)$$

The stress-energy of the plasma plus electromagnetic fields is of the form

$$T^{\mu\nu} = (\rho_m + p) u^\mu u^\nu + pg^{\mu\nu} + F^{\mu\alpha} F^{\nu\beta} g_{\alpha\beta} - \frac{1}{4} g^{\mu\nu} F^{\alpha\beta} F_{\alpha\beta}, \quad (26)$$

where ρ_m is the plasma mass density, p is the plasma pressure, u^α are the components of the plasma velocity field, and $F^{\mu\nu}$ are the components of the anti-symmetric field strength tensor. The trace condition then becomes

$$-16\pi E + 2\theta^2 + 16\pi ((N_z - v_s) J_z + 2N_x J_x) = 4\pi (\rho_m - 3p), \quad (27)$$

which on the stress-energy side involves only the massive fluid as the electromagnetic stress-energy is trace-less. Further, note that the energy and momentum conditions involve both the plasma and the electromagnetic fields

$$E = \rho_m (u^0)^2 + \frac{1}{2} E^i E_i - \frac{1}{2} (N_i E^i)^2 + \frac{1}{2} B^i B_i, \quad (28)$$

$$J_i = \rho_m u_i u^0 + \frac{1}{2} \epsilon_{ijk} E^j B^k, \quad (29)$$

where E^i are the components of the electric field and B^i are the components of the magnetic field. The trace equation is principally used to derive the motion of the soliton in the presence of a given fluid's mass and pressure density. For steady-state motion, the overall velocity of the soliton can be found

$$v_s = N_z + 2N_x \frac{J_x}{J_z} + \frac{1}{8\pi J_z} (\theta^2 - 8\pi E + 2\pi (\rho_m - 3p)) \quad (30)$$

and is seen to scale as a typical value of N_z . The value of v_s must be constant over all of space-time as the soliton motion is assumed to be steady state. The constant velocity can be arranged by the fluid mass and pressure density, each of which are positive definite. In their trace combination, $\rho_m - 3p$ can take on both positive and negative values, limited by the fluid equation of state. The most desirable velocity for the example soliton is consistent with the shift vector of the soliton's central region ($v_s = N_z(0, 0)$) and has trace that is consistent with a fluid whose equation of state is $p \leq \rho$, Fig. 6. In this case, the transportation properties of observers in the central region operate very similarly to solitons in the previous literature. Observers in the central region are found to travel along time-like curves with proper time rate matching

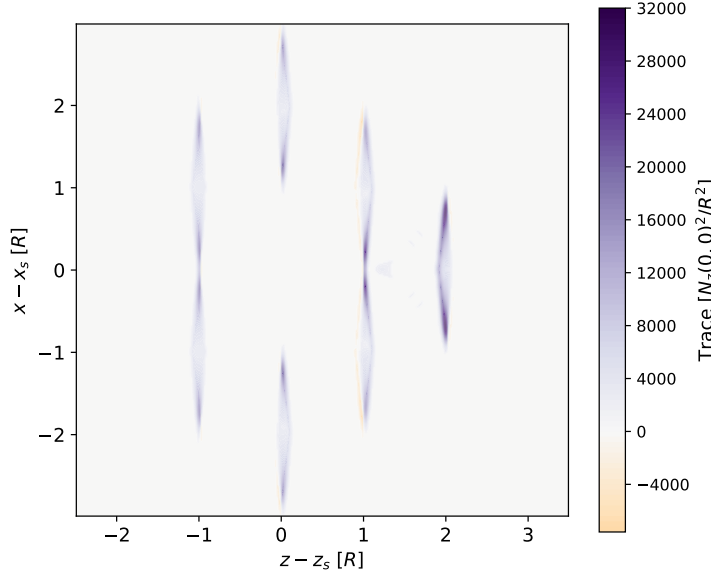


Figure 6. Projection of the Einstein tensor trace from Eqn. 27 along $(x, 0, z)$. Propagation of the soliton is taken to be uniform with speed consistent with shift vector in the central region, $v_s = N_z(0, 0)$.

those far from the soliton, $d\tau = dt$. The logistics of soliton travel then reflect those in [1].

In addition to supporting the energy, momentum, and trace conditions for steady-state motion, the plasma must satisfy its own conditions. These include the Maxwell equations for the electric and magnetic fields, the conservation and dynamical laws of the massive component of the plasma, the pressure equation of state, and the additional relations between the massive and electric current densities. These conditions are of sufficient number to determine all the plasma's degrees, meaning that the geometric conditions cannot in general be used to dictate the state of media without over-constraining it, as there is only one geometric degree and five non-trivial geometric conditions. To identify a solution of the more than dozen degrees of freedom of the plasma that satisfy the example soliton would require computation beyond the scope of this paper. What can be said here is that the conditions of the plasma are consistent with the soliton geometry. It is now a matter of finding the right configuration.

5. Conclusions

This paper has demonstrated that there exist superluminal solitons in general relativity satisfying both the weak energy condition and the momentum conditions for typical known sources of stress-energy. This is the first known solution of its kind, as previous superluminal solitons have required large amounts of negative energy. The positive-

energy geometries presented here distinguish themselves from the literature in that they obey a hyperbolic relation among their shift vector components in the form of a wave equation on the hypersurface, whereas only linear or elliptical relations had been previously considered. The solitons were further constructed to contain a central region with minimal tidal forces, where proper time coincides with asymptotic coordinate time, and any Eulerian observer within the central region would remain stationary with respect to the soliton. The transport logistics of the presented positive-energy solitons are similar to the solitons of the Alcubierre solution.

The energy and momentum conditions of the presented positive-energy geometries were found to conform to the expected range of a relativistic plasma. The trace of the Einstein equation, the single dynamical conditions that determines the hyperbolic shift vector potential, was used to determine the steady-state velocity of the soliton and was also found to be consistent with the plasma conditions. The geometric conditions on the plasma are deferential to the plasma's own dynamical equations, which include equations of motion and constitutive relations for both the massive fluid and the electromagnetic fields. The total energy requirements of the positive-energy solitons appear to be of the same order as the original Alcubierre soliton under the same shell-thickness-to-diameter conditions, with the energy for a soliton of modest radius $R = 100$ m and shell thickness $w = 1$ m requiring $E_{tot} \sim (\text{few}) \times 10^{-1} M_\odot v_s/c$. This energy, though still immense, is intriguing as there have been many advances in reducing the required energy of the negative-energy solitons that may be equally effective for this new class of solutions.

Future efforts can be divided into pursuits in theory and experiment. One could construct experimental or phenomenological methods to search for the signatures of positive-energy solitons in space–time. In experiment, for instance, one could augment existing interferometric searches [17, 22] to detect soliton space–time features from macroscopic plasmas as opposed to microscopic Casimir sources. The highly magnetized energetic and diffuse atmospheric plasma of magnetars could also be a natural place to look for signatures of positive-energy soliton geometries.

For theory, it is an appealing proposition to incorporate the degrees and dynamics of the plasma into the geometric computation. One could self-consistently simulate the creation, propagation, and dismantlement phases of a soliton at both sub- and superluminal speeds. Other directions include detailed optimizations of the solutions over energy and other trade-offs, the broadening the soliton geometry to incorporate a “payload” in the soliton’s central region, and studying the challenges of horizon formation when transitioning to superluminal speeds. However, developing models and configurations of the plasma alongside the geometry would in general require a large-scale numerical effort. Fortunately, in the era of gravitational-wave astronomy and high-precision cosmology, there exist a number of numerical relativity codes that are increasingly capable of describing massive fluids and gauge fields in relativistic space–time.

6. Acknowledgements

I would like to thank Katy Clough, Leslie Rosenberg, Andreas Karch, and Sanjay Reddy for their insightful comments during the preparation of this manuscript.

References

- [1] Alcubierre M 1994 *Classical and Quantum Gravity* **11** L73–L77 (*Preprint* [gr-qc/0009013](#))
- [2] Everett A E 1996 *Phys. Rev. D* **53**(12) 7365–7368 URL <https://link.aps.org/doi/10.1103/PhysRevD.53.7365>
- [3] Pfenning M J and Ford L H 1997 *Classical and Quantum Gravity* **14** 1743–1751 URL <https://doi.org/10.1088%2F0264-9381%2F14%2F7%2F011>
- [4] Hiscock W A 1997 *Classical and Quantum Gravity* **14** L183–L188 URL <https://doi.org/10.1088%2F0264-9381%2F14%2F11%2F002>
- [5] Krasnikov S V 1998 *Phys. Rev. D* **57**(8) 4760–4766 URL <https://link.aps.org/doi/10.1103/PhysRevD.57.4760>
- [6] Olum K D 1998 *Phys. Rev. Lett.* **81**(17) 3567–3570 URL <https://link.aps.org/doi/10.1103/PhysRevLett.81.3567>
- [7] Van Den Broeck C 1999 *Classical and Quantum Gravity* **16** 3973–3979 (*Preprint* [gr-qc/9905084](#))
- [8] Millis M G 1999 *Acta Astronautica* **44** 175 – 182 ISSN 0094-5765 missions to the Outer Solar System and Beyond URL <http://www.sciencedirect.com/science/article/pii/S0094576599000454>
- [9] Visser M, Bassett B and Liberati S 2000 *Nuclear Physics B - Proceedings Supplements* **88** 267 – 270 ISSN 0920-5632 URL <http://www.sciencedirect.com/science/article/pii/S0920563200007829>
- [10] Loup F, Waite D and Halerewicz E J 2001 *arXiv e-prints* gr-qc/0107097 (*Preprint* [gr-qc/0107097](#))
- [11] Natário J 2002 *Classical and Quantum Gravity* **19** 1157–1165 (*Preprint* [gr-qc/0110086](#))
- [12] Gauthier C, Gravel P and Melanson J 2002 *International Journal of Modern Physics A* **17** 2761
- [13] Lobo F and Crawford P 2003 *Weak Energy Condition Violation and Superluminal Travel* vol 617 p 277
- [14] Lobo F S N and Visser M 2004 *Classical and Quantum Gravity* **21** 5871–5892 URL <https://doi.org/10.1088%2F0264-9381%2F21%2F24%2F011>
- [15] Lobo F S N 2007 *arXiv e-prints* arXiv:0710.4474 (*Preprint* [0710.4474](#))
- [16] Obousy R K and Cleaver G 2008 *Journal of the British Interplanetary Society* **61** 364–369 (*Preprint* [0712.1649](#))
- [17] White H 2013 *Journal of the British Interplanetary Society* **66** 242–247
- [18] DeBenedictis A and Ilijić S 2018 *Classical and Quantum Gravity* **35** 215001 (*Preprint* [1807.09745](#))
- [19] Arnowitt R, Deser S and Misner C W 1959 *Phys. Rev.* **116**(5) 1322–1330 URL <https://link.aps.org/doi/10.1103/PhysRev.116.1322>
- [20] Misner C W, Thorne K and Wheeler J 1973 *Gravitation* (San Francisco: W. H. Freeman) ISBN 978-0-7167-0344-0, 978-0-691-17779-3
- [21] Bardeen J M and Piran T 1983 *Physics Reports* **96** 205 – 250 ISSN 0370-1573 URL <http://www.sciencedirect.com/science/article/pii/0370157383900698>
- [22] Lee J S and Cleaver G B 2016 *Physics Essays* **29** 201–206 (*Preprint* [1407.7772](#))